NASA Technical Memorandum 82666

Influence of Exit Impedance on Finite Difference Solutions of Transient Acoustic Mode Propagation in Ducts

K. J. Baumeister
Lewis Research Center
Cleveland, Ohio

Prepared for the
1981 Winter Annual Meeting of the American Society
of Mechanical Engineers
Washington, D.C., November 15-20, 1981

NASA

INFLUENCE OF EXIT IMPEDANCE ON FINITE DIFFERENCE SOLUTIONS OF TRANSIENT ACOUSTIC MODE PROPAGATION IN DUCTS

K. J. Baumeister
NASA Lewis Research Center
Cleveland, Ohio 44135

E-940

NOMENCLATURE

C_0^*	ambient speed of sound, m/sec
C_g^*	group velocity, m/sec
C_ϕ^*	phase speed, m/sec
f^*	frequency, Hz
H	unit step function, eqs. (22) and (23)
I	number of axial grid points
J	number of transverse grid points
J_m	Bessel function of order m
L^*	length of duct, m
m	spinning mode number
P	time-dependent dimensionless acoustic pressure, $P(x,r,t)$, $P^*/\rho_0^* C_0^{*2}$
P_m	time-dependent dimensionless acoustic pressure associated with m mode
$P_{m,n}$	analytical solution for m spinning mode and n radial mode
P'	time-depennent dimensionless acoustic pressure with angular variations, $P'(x,r,\theta,t)$, $P'^*/\rho_0^* C_0^{*2}$
p	spatially dependent "steady state" acoustic pressure, $P(x,r)$
r	radial coordinate, r^*/r_0^*
r_0^*	radius of duct, m
Δr	radial grid spacing
T^*	period, $1/f^*$, sec
t	dimensionless time, t^*/T^*
Δt	time step
U	axial acoustic velocity, U^*/C_0^*
x	axial coordinate, x^*/r_0^*
Δx	axial grid spacing
Z^*	acoustic impedance, kg/m^2 sec
$\alpha_{m,n}$	eigenvalue (n^{th} zero of $J_m'(\alpha)$)
β	eq. (12)
γ	eq. (21)
ζ	specific acoustic impedance, $Z^*/\rho_0^* C_0^*$
ζ_e	specific acoustic impedance at exit
ζ_∞	specific acoustic impedance of infinite duct
η_{cut}	cutoff frequency
η_r	dimensionless frequency, $r_0^* f^*/C_0^*$
θ	angular coordinate
λ	dimensionless axial wavelength

ξ cutoff ratio, η_r/η_{cut}

ρ_0^* ambient air density, kg/m^3

ω angular frequency

Subscripts:

e exit condition

i axial index (fig. 1)

j radial index (fig. 1)

m spinning mode number

n radial mode number

0 ambient condition

Superscripts:

* dimensional quantity

k time step

INTRODUCTION

With the introduction of strict aircraft noise regulations in the late 1960's the new aircraft nacelle designs required acoustic treatment in the inlet and exhaust ducts to reduce engine fan noise. To minimize the weight penalty of wall treatment, the aerospace industry has been concerned with reducing the length of a liner for a required sound attenuation. Analytical techniques are needed to handle sound propagation in ducts with axial variations in cross-sectional area or in wall liner impedance (absorbers) and with gradients in the flow Mach number. In an attempt to meet this need, both finite difference and finite element numerical techniques were developed.

At the present time both "steady state" and transient numerical theories have been applied to the problem of sound propagation in ducts. In the steady-state theory the pressure and acoustic velocities are assumed to be simple harmonic functions of time; thus the equations governing sound propagation (linearized gas dynamic equations) become independent of time. Generally the steady-state finite difference and finite element numerical algorithms have been limited to low frequency and short ducts because of the large matrices associated with the solutions of the time-independent equations. For a listing of recent publications and more details on the techniques and problems associated with the numerical solutions of the sound propagation equations, refer to reference 1, which contains a comprehensive literature summary covering both finite difference and finite element analysis of small-amplitude (linear) sound propagation in straight and variable-area ducts.

As an alternative to the previously developed steady-state theories, time-dependent numerical solutions were developed for plane-wave noise propagation in a two-dimensional rectangular duct without flow (ref. 2), for parallel sheared mean flow (ref. 3), and for higher order mode propagation in a cylindrical duct with a uniform mean flow (ref. 4). Advantageously matrix storage requirements are completely eliminated in the time-dependent analysis. Only the solution vectors for pressure and velocity need be stored. Thus the transient solutions can easily be applied in long ducts and in high-frequency applications, such as in the inlet of a turbofan engine.

At the present time, however, the transient method appears to have one major drawback. The transient method, as formulated in reference 4, does not converge for cutoff acoustic modes. This has implications as to its use in a variable area where modes may become cutoff in the small-area portion of the duct. When a single acoustic mode begins to move along a variable-area duct, part of its energy will be continuously transferred to the other duct modes (ref. 5). If the initial mode is near cutoff, significant energy could be transferred to a cutoff mode. Also, when abrupt changes in geometry or wall impedance occur in a duct, a full range of acoustic modes (including cutoff) is required to match pressure and velocity across the interface (ref. 6). Consequently the purpose of the present paper is to resolve the stability problem associated with the transient calculation of cutoff acoustic modes.

The numerical analysis to follow models the closed-form pressure solutions for cutoff and propagating acoustic modes in a semi-infinite duct. The first section of the paper presents the various equations and boundary conditions governing sound propagation in a duct without a mean flow. The second section then presents the difference form of the governing equations. Next analytical approximations (steepest descent) are presented as a guide to the understanding of the numerical results that follow. Numerical calculations are presented at forcing frequencies above, below, and nearly at the cutoff frequency. At that time an explanation is presented for the computational instability associated with cutoff modes. Finally recommendations are made on how to handle cutoff mode propagation.

GOVERNING EQUATIONS AND BOUNDARY CONDITIONS

The propagation of sound in an axisymmetric, cylindrical, hard-wall duct, as shown in figure 1, is described by the wave equation and appropriate impedance boundary conditions.

Wave Equation

The wave equation is a circular duct without a mean flow can be expressed in dimensionless form as

$$\frac{\partial^2 p'}{\partial x^2} + \frac{\partial^2 p'}{\partial r^2} + \frac{1}{r}\frac{\partial p'}{\partial r} + \frac{1}{r^2}\frac{\partial^2 p'}{\partial \theta^2} = \eta_r^2 \frac{\partial^2 p'}{\partial t^2} \qquad (1)$$

These and other symbols are defined in the nomenclature. The dimensionless frequency η_r is defined as

$$\eta_r = \frac{r_0^* \omega^*}{2\pi c_0^*} = \frac{r_0^* f^*}{c_0^*} \qquad (2)$$

The asterisks denote dimensional quantities.

Because of the rotational nature of the rotor blades on a typical turbofan jet engine, large circumferential variations in acoustic pressure will occur depending on blade number and engine rpm. A three-dimensional solution for sound propagation, however, would be expensive to perform. Customarily, since the equations are linear, the circumferential acoustic pressure variations are decomposed into spinning modes m:

$$P'(x,r,\theta,t) = \sum_m P_m(x,r,t)e^{im\theta} \qquad (3)$$

The summation is over those modes that are present in a particular application. Considering solutions with a single spinning mode number m

$$P'(x,r,\theta,t) = P(x,r,t)e^{im\theta} \qquad (4)$$

the wave equation (1) reduces to

$$\frac{\partial^2 p}{\partial x^2} + \frac{\partial^2 p}{\partial r^2} + \frac{1}{r}\frac{\partial p}{\partial r} - \frac{m^2}{r^2}p = \eta_r^2 \frac{\partial^2 p}{\partial t^2} \qquad (5)$$

Equation (5) in difference form will be solved to determine the pressure in the duct

Hard-Wall Boundary Condition

The boundary condition at the surface of a hard-wall duct is

$$\frac{\partial p}{\partial r} = 0 \qquad (6)$$

Entrance Condition

The boundary condition at the source plane $P(0,r,t)$ will be assumed to vary as $e^{i\omega^* t^*}$ or in a dimensionless form as $e^{i2\pi t}$. Furthermore the transverse pressure variation (r direction) will be assumed to correspond to the eigenfunctions $J_m(\alpha_{mn}r)$ associated with mode propagation in an infinitely long hard-wall duct. The eigenvalues associated with mode m,n are tabulated in reference 7 (p. 511) and reference 8 (p. 411). Therefore the source boundary condition used herein is

$$P(0,r,t) = J_m(\alpha_{mn}r)e^{i2\pi t} \qquad (7)$$

Exit Impedance

The boundary condition at the exit of the duct can be expressed in terms of a specific acoustic impedance defined as

$$\zeta_e = \frac{p}{U} \qquad (8)$$

where the equation describing the acoustic velocity U is

$$\frac{\partial U}{\partial t} = -\frac{1}{\eta_r}\frac{\partial p}{\partial x} \qquad (9)$$

Substituting equation (8) into equation (9) yields

$$\frac{\partial p}{\partial x} = -\frac{\eta_r}{\zeta_e}\frac{\partial p}{\partial t} \qquad (10)$$

In reference 4, ζ_e has been assumed to be the steady-state impedance associated with mode propagation down an infinite duct. For transmission of a single acoustic mode without reflection, the exit impedance is

$$\zeta_e = \frac{1}{\beta} \qquad (11)$$

where

$$\beta = \sqrt{1 - \left(\frac{\alpha_{mn}}{2\pi\eta_r}\right)^2} \quad \text{for} \quad \eta_r > \frac{\alpha_{mn}}{2\pi} \qquad (12)$$

for propagating modes and

$$\beta = -i\sqrt{\left(\frac{\alpha_{mn}}{2\pi\eta_r}\right)^2 - 1} \quad \text{for} \quad \eta_r < \frac{\alpha_{mn}}{2\pi} \qquad (13)$$

for cutoff acoustic modes. The negative root is required for damping when $e^{+i\omega^* t^*}$ is assumed to be the forcing function.

All the other equations and boundary conditions are exact. The exit impedance ζ_e was the only condition that was modeled in an approximate manner. As indicated by its title, this paper concentrates on exact treatment of the exit impedance condition.

Centerline Condition

For plane-wave propagation (m = 0, n = 0), $\partial P/\partial r$ is zero at the centerline; for modes with m equal to or greater than 1, $P(x,0,t)$ is zero. Also $\partial P/\partial r$ is zero for m greater than 1.

Initial Condition

For times equal to or less than zero the duct is assumed to be quiescent; that is, the acoustic pressures and velocities are taken to be zero. For times greater than zero the application of the noise source (eq. (7)) will drive the pressure in the duct.

DIFFERENCE EQUATIONS

Instead of a continuous solution in space and time the finite-difference approximations will determine the pressure at isolated grid points in space as shown in figure 1 and at discrete time steps Δt. Starting from the known initial conditions at $t = 0$ and the boundary conditions, the finite-difference algorithm will march out the solution to later times. No special starting equation will be required, because both the pressure and acoustic velocities are initially assumed to be zero, a quiescent duct.

Difference Equations

Away from the duct boundaries, in cell 1 of figure 1, the first and second derivatives in the wave equation (eq. (5)) can be represented by the usual central differences in time and space (ref. 9, p. 452)

$$\left(\frac{p^k_{i+1,j} - 2p^k_{i,j} + p^k_{i-1,j}}{\Delta x^2}\right) + \left(\frac{p^k_{i,j+1} - 2p^k_{i,j} + p^k_{i,j-1}}{\Delta r^2}\right) + \frac{1}{r_j}\left(\frac{p^k_{i,j+1} - p^k_{i,j-1}}{2\Delta r}\right) - \frac{m^2}{r_j^2}p^k_{i,j} = \eta_r^2\left(\frac{p^{k+1}_{i,j} - 2p^k_{i,j} + p^{k-1}_{i,j}}{\Delta t^2}\right) \qquad (14)$$

where i and j denote the space indices; k the time index; and Δx, Δr, and Δt the space and time mesh spacings, respectively.

Equation (14) can be rewritten as

$$p^{k+1}_{i,j} = 2p^{k}_{i,j} - p^{k-1}_{i,j} + \left(\frac{\Delta t}{\eta_r \Delta r}\right)^2 \left[\left(\frac{\Delta r}{\Delta x}\right)^2 p^{k}_{i-1,j} + \left(1 - \frac{\Delta r}{2r_j}\right) p^{k}_{i,j-1} - 2\left[1 + \left(\frac{\Delta r}{\Delta x}\right)^2 + \frac{1}{2}\left(\frac{m\Delta r}{r_j}\right)^2\right] p^{k}_{i,j} + \left(1 + \frac{\Delta r}{2r_j}\right) p^{k}_{i,j+1} + \left(\frac{\Delta r}{\Delta x}\right)^2 p^{k}_{i+1,j}\right] \quad (15)$$

Equation (15) is an algorithm that permits marching out solutions from known values of pressure at times associated with k and k - 1. The difference equations for cells 2 to 6 in figure 1 are of slightly different form. These equations as well as their derivations are given in references 2 and 4.

Spatial Mesh Size

The mesh spacings Δx and Δr must be restricted to small values to reduce the truncation error. To resolve the oscillatory nature of the acoustic pressure, the required number of grid points I in the axial direction and J in the r direction were given in reference 4 as

$$I \geq 12\, \eta_r \frac{L^*}{r_0^*} \beta \quad (16)$$

$$J \geq 12\, \eta_r \quad (17)$$

Stability

In the explicit time-marching approach used here roundoff errors can grow in an unbounded fashion and destroy the solution if the time increment Δt is too large or if the iteration scheme is improperly posed. For spinning wave propagation in a thin annulus the Von Neumann method (ref. 10) applied to equation (14) yields

$$\Delta t \leq \frac{\eta_r \Delta r}{\left[1 + \left(\frac{\Delta r}{\Delta x}\right)^2 + \left(\frac{m\Delta r}{2}\right)^2\right]^{1/2}} \quad (18)$$

For circular ducts Δt was empirically decreased by a factor of 0.5.

ANALYTICAL SOLUTION

The wave equation (1) and its associated boundary and initial conditions can be solved directly for the semi-infinite duct shown in figure 2(a) by the use of the Laplace transform (ref. 5). To obtain a more useful solution, Pearson (ref. 5) has also solved equation (1) by the method of steepest decent to obtain

$$\frac{P(x,r,t)}{e^{12\pi t}} = H(t - \eta_r x) \left\{\begin{matrix}\text{transient}\\ \text{solution}\end{matrix}\right\} + H\left(t - \frac{\eta_r x}{\beta}\right) J_m(a_{mn} r)\, e^{-12\pi \eta_r \beta x} \quad \text{for } \eta_r > \frac{a_{mn}}{2\pi} \quad (19)$$

$$\frac{P(x,r,t)}{e^{12\pi t}} = H(t - \eta_r x) \left\{\begin{matrix}\text{transient}\\ \text{solution}\end{matrix}\right\} + H\left(t - \frac{\eta_r x}{\gamma}\right) J_m(a_{mn} r)\, e^{-a_{mn}\gamma x} \quad \text{for } \eta_r < \frac{a_{mn}}{2\pi} \quad (20)$$

where H is the unit step function and

$$\gamma = \sqrt{1 - \left(\frac{2\pi\eta_r}{a_{mn}}\right)^2} \quad (21)$$

The functional form of the transient solution is presented later.

In reference 5 the duct eigenfunctions were left in a general form. Herein the cylindrical form of the eigenfunction is used, and the original equations of reference 5 are rewritten in a dimensionless form. Also, only the real part of the transient and steady-state solutions was presented in reference 5. These solutions, however, are presented in complex form in equations (19) and (20). Because the transient terms correspond to waves that are propagating but are not simple harmonic in nature, the usual restriction that cutoff waves do not carry energy (ref. 11, p. 53) does not apply during the transient.

As a result of the method of steepest decent the acoustic pressure field inside the duct is split into a transient motion and a steady-state solution that is either propagated (eq. (19)) or attenuated (eq. (20)) depending on whether the frequency of the forcing field is greater or less than the cutoff frequency of the mode considered. The steady-state solution is also the solution to equation (1) when the pressure is assumed to be a simple harmonic function of time.

For propagating modes the physical significance of the unit step functions in equation (19) can best be described if they are rewritten in dimensional form:

$$H(t - \eta_r x) = H\left(t^* - \frac{x^*}{c_0^*}\right) \quad (22)$$

and

$$H\left(t - \frac{\eta_r x}{\beta}\right) = H\left(t^* - \frac{x^*}{c_g^*}\right) \quad (23)$$

Thus the transient term in equation (19) travels at the signal velocity (ref. 7, p. 479) which is the speed of sound of the medium. The transient front is defined as the surface beyond which the medium is completely at rest at any given instant of time. On the other hand the steady-state solution travels at the group velocity C_g^*, which is simply

$$C_g^* = \frac{C_0^{*2}}{C_\phi^*} \tag{24}$$

where C_ϕ^* is the common phase velocity (ref. 7, p. 498) defined for steady-state solutions. The phase velocity C_ϕ^* is always greater than C_0^*; the group velocity is always less than C_0^*.

SIMULATION OF SEMI-INFINITE DUCT

The form of the transient solution leads to some observations that are pertinent to the numerical results to follow. First, the time in which to perform the transient solution increases near the cutoff frequency. In fact, equation (23) indicates that a mode exactly at cutoff can never exist at steady state since its group velocity is zero. Second, the impedance at any position will not be equal to the steady-state impedance during the initial transient. Thus equation (11) is not the exact analytical condition for no reflections during the transient. As a consequence of using equation (11) during the transient, part of the acoustic energy reaching the exit will be reflected back toward the source.

For modes with small group velocities near the cutoff frequency, the possibility exists that the use of equation (11) as a boundary condition could introduce an unstable feedback loop into the numerical analysis. This computational instability could prevent the establishment of the true steady-state solution. Therefore the possibility that the exit impedance was the cause of the instability of cutoff acoustic modes (ref. 4), as discussed in the introduction, is now investigated.

The present analysis attempts to numerically reproduce the steady-state analytical solutions given by equations (19) and (20) for the acoustic pressure in the domain $0 \le x \le 1$ in the semi-infinite duct of figure 2(a). A variety of frequencies above and below the cutoff frequency are chosen. In the numerical simulation a finite-length duct ($L^*/r_0^* = 1$), shown in figure 2(b), and a long duct ($L^*/r_0^* = 40$), shown in figure 2(c), are used. The latter case exactly simulates an infinite duct if the numerical calculations are terminated before the return of the initial reflected wave from the duct exit.

DISCUSSION OF RESULTS

In this section the calculated axial pressure profile of the 3,0 mode is examined at frequencies above, below, and nearly at the cutoff frequency. In these problems the time-dependent numerical results are compared with the exact solutions given by the second term in equations (19) and (20). The stability of the numerical solutions is examined for source frequencies near the cutoff frequency.

In the numerical computer program the values of pressure are calculated at each grid point i,j for each time step k. Only the values of pressure at times k and $k-1$ need to be stored since only the pressures at the two previous time steps are needed for the p^{k+1} calculation (eq. (15)). After sufficient time has passed so that the steady-state solution has traveled to the position $x = 1$, ($H(t - \eta_r/\beta)$ or $H(t - \eta_r/\gamma) = 1$) and after an additional time period elapses such that the transient terms have died out (checked numerically), the time-dependent results can be compared with the steady-state results. In this comparison the time-dependent pressure is simply divided by $e^{i2\pi t}$ to obtain

$$p = \frac{P(x,r,t)}{e^{i2\pi t}} \tag{25}$$

which represents a numerical approximation to the Fourier transform of $P(x,r,t)$ as stated in reference 12 (p. 11).

In all the cases to be examined now the numerical and analytical pressure profiles are displayed for the domain $0 \le x \le 1$ for a hard-wall, semi-infinite duct with an $m=3$ spinning mode and the lowest order radial eigenvalue ($\alpha_{3,0} = 4.20119$). The values of the acoustic pressure are displayed at $r = 1$, along the duct wall. Also, to keep the graphical displays simple, only the real components of pressure are compared.

The ratio of the forcing frequency η_r to the cutoff frequency η_{cut} is defined as ξ. For the $m=3$ spinning mode, the cutoff frequency is $\eta_{cut} = 0.66864$. Therefore

$$\xi = \frac{\eta_r}{0.66864} \tag{26}$$

Finally, in the discussion to follow, the ratio of the speed of sound to the group velocity C_0^*/C_g^* is cited. This ratio is equal to the dimensionless time t required for the steady-state solution to propagate to the $x=1$ position in the duct. This parameter is also used as a measure of how close the forcing frequency is to the cutoff frequency. The difference in the calculated time t and the ratio C_0^*/C_g^* represents the added computational time required for the transient terms to die out so that the steady-state terms become dominant.

Propagating Acoustic Modes

The numerical and analytical profiles are compared in figure 3 for $\eta_r = 1$. In this case the ratio of sonic to group velocity C_0^*/C_g^* is 1.345 ($\xi = 1.5$). As shown in figure 3, at $t = 1.86$ the analytical and the numerical results for both the short duct (fig. 2(b)) and the long duct (fig. 2(c)) are in good agreement.

For a source frequency nearer to cutoff, $\eta_r = 0.7$ ($\xi = 1.047$ with $C_0^*/C_g^* = 2.365$), the time required to obtain a steady-state solution increases to 6 for the long duct and 10 for the short duct. Again, the numerical solutions converge to the analytical solutions, as shown in figure 4. Further improvement between the numerical and analytical solutions could be obtained by using more axial grid points (smaller Δx).

To illustrate the temporal nature of the acoustic signal, the time history of the acoustic pressure at the axial position $x = 1$ and at the duct wall ($r = 1$) is presented in figure 5. In figure 5 the solid line represents the steady-state solution, which is cut on when $H(t - \eta_r x/\beta)$ becomes 1. The

solid line is calculated from the last term in equation (19).

The dashed line in figure 5 represents the steepest-descent analytical approximations for the transient pressure terms in equations (19) and (20). The real part of the transient acoustic pressure was derived in reference 5 from Debye's formula. In dimensionless form the real part of the transient term is

$$\begin{Bmatrix} \text{real} \\ \text{transient} \\ \text{solution} \end{Bmatrix} \sim -\left(\frac{2\eta_r}{\pi a_{mn}}\right)^{1/2} \times \frac{H(t-\eta_r x)\, x\, a_{mn}^2 \cos\left[a_{mn}\left(t^2/\eta_r^2 - x^2\right)^{1/2} - \pi/4\right]}{\eta_r\left(t^2 - x^2\eta_r^2\right)^{1/4}\,(2\pi\beta)^2\left\{t^2 - x^2\eta_r^2/\beta^2\right\}} \tag{27}$$

Equation (27) applies to both equations (19) and (20). The Debye form of the steepest-descent approximation has a singularity at the time of arrival of the transient ($t = \eta_r x$) and at the arrival of the steady-state solution ($t = \eta_r x/\beta$). Consequently the steetest-descent solutions are compared with the exact numerical results away from these two singular points. A gap in the steepest-descent solution (dashed line) is left in figure 5 about the singular points.

The circular symbols in figure 5 represent the numerical finite difference calculations. Because the numerical time increments are chosen small for numerical stability, errors in the numerical solution can arrive slightly ahead of the acoustic wave. However, these errors are quite small.

For the forcing frequency $\eta_r = 0.7$, as shown in figure 5, the transient arrives at position $x = 1$ when $t = 0.7$; the steady-state signal arrives at $t = 2.36$. In general, as shown in figure 5 the numerical and analytical theories are in reasonable agreement. The transient term tends to suppress the peaks of the temporal acoustic signal during the initial portion of the transient. By a dimensionless time of 7.0, however, the transient has died out.

Next a numerical solution was obtained for a forcing frequency $\eta_r = 0.0087$ ($\xi = 1.00009$) with a c_0^*/c_g^* ratio of 50. In this case the numerical results for only the short duct (fig. 2(b)) are displayed. As shown in figures 3 and 4 the use of a steady-state impedance exit condition leads to convergence to the steady-state solution.

For the short duct, as shown in figure 6, convergence between the numerical and analytical results is obtained even very close to the cutoff frequency. In this case the dimensionless time for convergence is extremely long. In a sense these numerical results have validated the results of the steepest-descent approximation to the transient duct propagaton problem. By a mental extrapolation, for a forcing function at the cutoff frequency, the concept of an infinite time to set up steady-state conditions seems plausible. This discontinuity in group velocity at the cutoff frequency could be significant in transient-mode measuring schemes, such as in reference 13.

Finally, for ξ greater than 1, the use of a steady-state exit impedance does not affect convergence even in the extreme case of large c_0^*/c_g^* values.

Nonpropagating Acoustic Modes

Acoustic modes with forcing frequencies below their cutoff frequency are said to be nonpropagating because their time-averaged, steady-state acoustic intensity is zero (ref. 11, p. 53). The pressure fields, however, do propagate down the duct according to equation (20).

For the 3,0 acoustic mode at a forcing frequency η_r of 0.6 ($\xi = 0.9$), the steady-state energy is nonpropagating. The dimensionless time required for the steady-state pressure to reach $x = 1$ is 1.359. The numerical and analytical profiles for this mode are compared in figure 7 for the exit impedance condition shown in figure 2(a). As shown in figure 7 the numerical values of the acoustic pressure did not converge to the analytical values, even when the calculational time was extended to 120. This was the computational stability problem alluded to in reference 4.

On the other hand, when the same calculation was performed for the $L^*/r_0^* = 40$ duct, the numerical calculations quickly converged to the analytical results, as shown in figure 8. Therefore the conclusion was drawn that the assumption of a steady-state impedance at $x = 1$ causes a finite-amplitude instability in the numerical solutions.

In contrast to the case of a propagating mode such as shown in figure 6, for cutoff modes the transient component initially dominates the steady-state component of pressure because the steady-state component is damped by $e^{-a_{mn}Y_R}$. Figure 9 illustrates the relatively larger magnitude of the transient component of pressure as compared with the steady state over the first three time periods. As shown in figure 9 the analytical solution (dashed line) is in reasonable agreement with the numerical results.

Most likely, because the steady-state impedance is completely reactive (eqs. (11) and (13)) for steady-state cutoff modes, none of the acoustic energy associated with the dominant transient solution can escape the duct. Recall that, when a steady-state wave impinges on a purely reactive plane, the magnitude of the reflection coefficient is unity (ref. 7, p. 262). Or conversely, the steady-state power radiated from a plane surface is proportional to resistance (ref. 14, p. 247), which is zero for the cutoff mode. Although we are not dealing with a steady-state wave, the use of a purely imaginary exit impedance could induce large reflections of the transient power, which would prevent the obtaining of a steady-state condition in a transient analysis. In contrast, in the conventional steady-state numerical analysis, the use of a purely reactive exit impedance is acceptable (ref. 15, fig. 5).

Clearly steady-state exit impedances cannot be used in a transient study of cutoff acoustic modes. In general a steady-state exit impedance should only be used as an approximation for the duct exit terminaton for a single propagating acoustic mode.

Up to this point the exit impedance employed has been associated with a single propagating acoustic mode in a hard-wall duct. However, the exact exit impedance is unknown for multimode (including cutoff modes) transient propagation in straight soft-wall and hard-wall ducts with axially varying area. Some general procedures for overcoming the difficulties of multimode exit conditions are discussed in the following section on exit impedance models.

EXIT IMPEDANCE MODELS

In applying the finite difference or finite element analysis to an actual engine inlet, the grid system has generally been confined to the internal portion of the engine. Thus the engine has been modeled as a short pipe. In this case an exit impedance is chosen at the inlet face or jet exhaust plane. However, the internal grid structure may be extended into the far field, in which case a far-field exit impedance would be employed. First, some possible ways to choose the impedance at the engine exits are discussed. Next, the advantages and procedures for moving the exit impedance plane into the far field are presented.

A problem often encountered in inlet design is the determination of the optimum attenuation of one or more soft-wall (absorbing) liners. Figure 10(a) shows a simple straight-duct model of a turbojet inlet that is assumed to have two different values of wall impedance (absorbers) in series. For a fixed spinning mode number m, the acoustic pressure at the inlet face will be composed of many radial modes that propagate down the duct.

If a single radial mode is assumed at $x = 0$ in figure 10(a), the infinite hard-wall-duct impedance associated with this mode (eqs. (11) and (12)) would be an appropriate assumption. Generally only propagating modes at $x = 0$ would be used; therefore the purely imaginative exit impedances associated with cutoff modes would not be employed.

Because some modal scattering will generally occur at the various changes in wall impedance (ref. 16), many modes will actually be present at the duct exit. In the prediction of sound attenuation in these cases, the single impedance used in the numerical calculation (refs. 17 and 18) has been found to be in good agreement with the more exact analytical models (refs. 19 and 16). Apparently, by absorption the soft wall prevents the reflected waves from significantly affecting the acoustic field in the duct.

Reference 17 (appendix E, eq. (E10)) suggests another possibility for more accurately simulating a nonreflecting interface at the duct exit. By increasing the length of the last section (fig. 10(b)) the reflections from the duct exit will be effectively damped before they can reenter the original portion of the duct. The actual attenuation of the duct would be determined from pressures and velocities at the original duct exit shown by the dashed line in figure 10(b). Because of these large attenuations cutoff would not be a problem.

The additional damping impedance could also be added downstream of the exit, as shown in figure 10(c). The programmer might wish to consider some hard-wall section (variable area perhaps) added to the exit of liner Z_2. In this case, the possibility of model reflections at the entrance plane of the liner Z_3 could complicate the problem.

Finally, as discussed in this paper, reflections at the duct exit could be eliminated by simply extending the duct, as shown in figure 10(d), to large lengths, such that the calculation is performed prior to the return of the reflected wave. However, this could be expensive from the standpoint of computer storage and run times.

All the previous cases attempted to eliminate or at least reduce reflections at the duct exit. However, in the actual turbofan inlet or exhaust termination, reflections could be important for certain modes. Consequently continuing the grid structure from inside the nacelle into the far field would simulate the actual dynamic process occurring at the engine lip.

In the far field many of the problems discussed earlier are eliminated. For example, in the absence of a solid wall boundary condition, all modes propagate in the far field (ref. 12, p. 212). Therefore, in establishing the exit boundary condition in the far field, the problem of a cutoff mode computational instability is eliminated. Also, all the various duct modes have the identical $\rho_0^* c_0^*$ exit impedance far from the exit, which simplifies the exit condition even further.

In the far field the duct exit impedance would be applied along a spherical surface, as indicated by the dashed line shown in figure 11(a). For a harmonic diverging spherical wave (ref. 20, p. 80) or far from the face of a flat piston in an infinite wall (ref. 21, p. 168), the far-field acoustic impedance is

$$\zeta = \frac{1}{1 + \frac{1}{(2\pi\eta_r r)^2}} + \frac{i}{(2\pi\eta_r r) + \frac{1}{2\pi\eta_r r}} \qquad (28)$$

In equation (28), if r is assumed to be large, the limit is

$$\zeta = 1 \quad (Z = \rho_0^* c_0^*) \qquad (29)$$

In applying the transient technique to the configuration shown in figure 11(a), the method of mapping could be used. In particular, the mapping procedure developed by Thompson, et al. (ref. 22) provides for the automatic generation of a general coordinate system with coordinate lines coincident with all the boundaries of an arbitary shaped duct. This coordinate mapping procedure could be extended to the case of the external impedance condition shown in figure 11(a). An initial effort has resulted in the development of the appropriate transformed acoustic equations for a variable-area duct (ref. 23) for which theory and experimental data are in good agreement.

Another approach to establishing the impedance boundary condition is shown in figure 11(b). In this case a simple cylindrical geometry is used to enclose the exit of the duct. This has the advantage of allowing the use of the same rectangular array of grid points used in the interior of the duct, as shown in figure 1. Converting the radiation boundary condition for a sphere to a cylindrical boundary is discussed in reference 24. The authors also discuss a version of the exit impedance that could satisfy the no-reflection condition for more than one mode in a duct. In addition, reference 24 contains a comprehensive literature summary of recent work on the external radiation boundary condition.

CONCLUSIONS

The cutoff mode instability problem associated with a transient finite difference solution to the wave equation has been explained. The commonly used "steady state" impedance boundary condition was found to produce acoustic reflections during the initial transient. These reflections caused finite instabilities in the cutoff modes. Extending the duct length to prevent transient reflections resolved this stability problem. In addition, exit

impedance models are presented for use in the practical design of turbofan inlets.

With the resolution of the cutoff mode instability problem, the time-dependent analysis appears to be ideally suited to handle all aspects of numerical acoustic analysis. Recall that the time-dependent analysis does not require large matrix storage as do the steady-state finite difference and finite element techniques. Also, because manipulation of matrices is omitted, the time-dependent approach is relatively easy to program and debug.

REFERENCES

1 Baumeister, K. J., "Numerical Techniques in Linear Duct Acoustics - A Status Report," ASME Paper 80-WA/NC-2, Nov. 1980.

2 Baumeister, K. J., "Time Dependent Difference Theory for Noise Propagation in a Two-Dimensional Duct," AIAA Journal, Vol. 18, No. 12, Dec. 1980, pp. 1470-1476.

3 Baumeister, K. J., "A Time Dependent Difference Theory for Sound Propagation in Ducts with Flow," 98th Meeting of the Acoustical Society of America, Salt Lake City, UT, Nov. 26-30, 1979. (also NASA TM-79302, 1979).

4 Baumeister, K. J., "Time Dependent Difference Theory for Sound Propagation in Axisymmetric Ducts with Plug Flow," AIAA Paper No. 80-1017, June 1980.

5 Pearson, J. D., "The Transient Motion of Sound Waves in Tubes," Quarterly Journal of Mechanics and Applied Mathematics, Vol. VI, Pt. 3, Sep. 1953, pp. 313-335.

6 Beckemeyer, R. J. and Sawdy, D. T., "Boundary Conditions for Mode-Matching Analysis of Coupled Acoustic Fields in Ducts," AIAA Paper No. 78-194, Jan. 1978.

7 Morse, P. M. and Ingard, K. U., Theoretical Acoustics, McGraw Hill, New York, 1968.

8 Abramowitz, M. and Stegun, I. A., eds., Handbook of Mathematical Functions with Formulas, Graphs and Mathematical Tables, United States National Bureau of Standards, Washington, DC, Mathematics Series-55, 1964.

9 Gerald, C. F., Applied Numerical Analysis, 2nd ed., Addison-Wesley, Reading, MA, 1978.

10 Clarr, M. and Hansen, K. F., Numerical Methods of Reactor Analysis, Academic Press, New York, 1964.

11 Richards, E. J. and Mead, D. J., Noise and Acoustic Fatigue in Aeronautics, Wiley, New York, 1968.

12 Goldstein, M. E., Aeroacoustics, McGraw-Hill, New York, 1976.

13 Cicon, D. E., Sofrin, T. G., and Mathews, D. C., "Improved Methods for Fan Sound Field Determination," PWA-5635-43, Pratt and Whitney Aircraft Group, East Hartford, CT, Jan. 1981. (NASA CR-165188.)

14 Morse, Philip M., Vibration and Sound, 2nd ed., McGraw-Hill, New York, 1948.

15 Tag, I. and Lumsdaine, E., "An Efficient Finite Element Technique for Sound Propagation in Axisymmetric Hard Wall Ducts Carrying High Subsonic Mach Number Flows," AIAA Paper No. 78-1154, July 1978.

16 Sawdy, D. T., Beckemeyer, R. J., and Patterson, J. D., "Analytical and Experimental Studies of an Optimum Multisegment Phased Liner Noise Suppression Concept," 03-9812-1, Boeing Co., Wichita, KS, May 1976. (NASA CR-134950.)

17 Baumeister, K. J. and Bittner, E. C., "Numerical Simulation of Noise Propagation in Jet Engine Ducts," NASA TN D-7339, 1973.

18 Baumeister, K. J., "Evaluation of Optimized Multisectioned Acoustic Liners," AIAA Journal, Vol. 17, No. 11, Nov. 1979, pp. 1185-1192.

19 Rice, Edward J.: Attenuation of Sound in Softwalled Circular Ducts, AFOSR-UTIAS Symposium on Aerodynamic Noise, Tornoto, Canada, 1968, pp. 229-249.

20 Seto, W. W., Schaum's Outline of Theory and Problems of Acoustics," Schaum's Outline Series-495, McGraw-Hill, New York, 1971.

21 Kinsler, L. E. and Frey, A. R., Fundamentals of Acoustics, Wiley, New York, 1950.

22 Thompson, J. F., Thames, F. C., and Mastin, C. W., "Automatic Numerical Generation of Body-Fitted Curvilinear Coordinate System for Field Containing Any Number of Arbitary Two-Dimensional Bodies," Journal of Computational Physics, Vol. 15, July 1974, pp. 299-319.

23 White, J. W. "A General Mapping Procedure for Variable Area Duct Acoustics, AIAA 81-0094, Jan. 1981.

24 Bayliss, A. and Turkel, E., "Radiation Boundary Conditions for Wave-Like Equations," Communications of Pure and Applied Mathematics, Vol. 33, Nov. 1980, pp. 707-725.

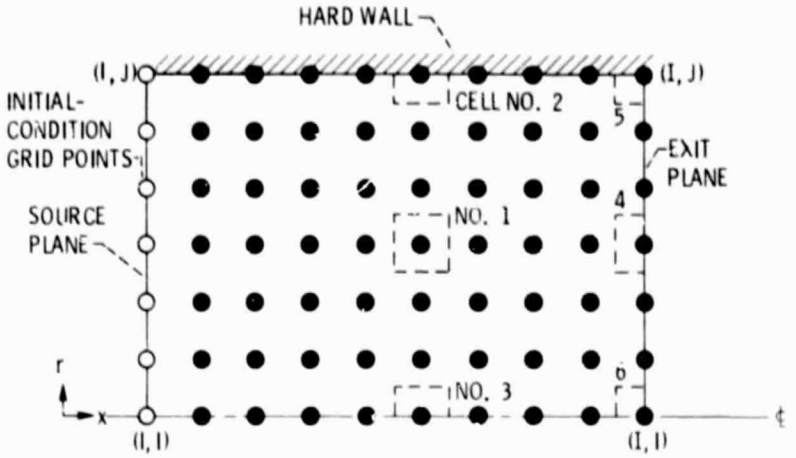

Figure 1. - Grid-point representation of cylindrical flow duct.

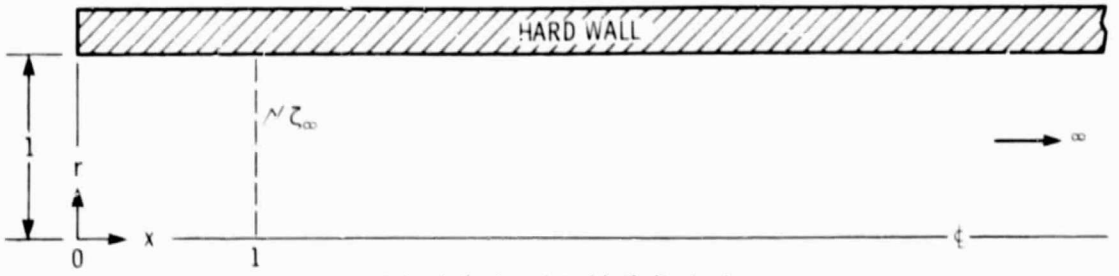

(a) Analytical model of infinite duct.

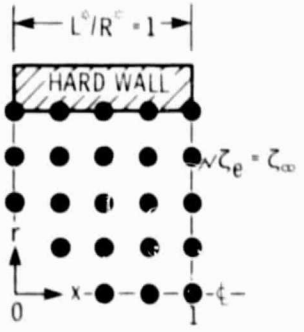

(b) Finite numerical representation of infinite duct for $x \leq 1$.

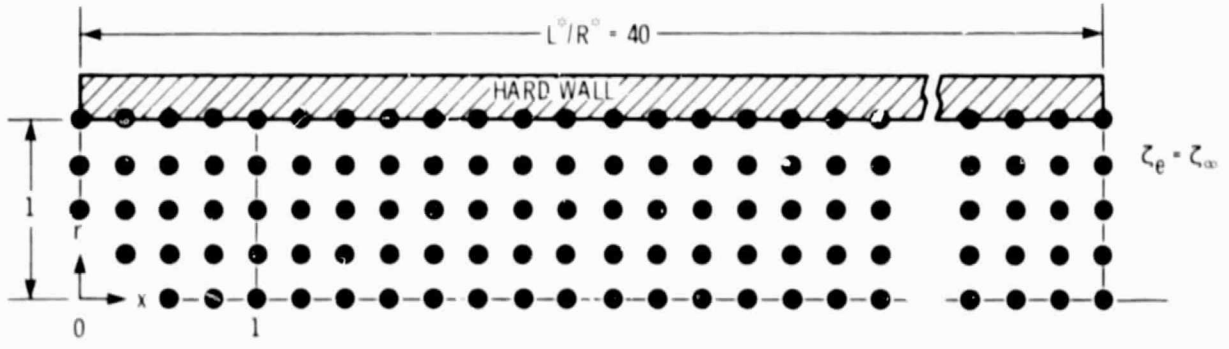

(c) Numerical approximation of infinite duct ($L^\circ/R^\circ = 40$).

Figure 2. - Numerical grid structure for representation of acoustic mode propagation in an infinite duct.

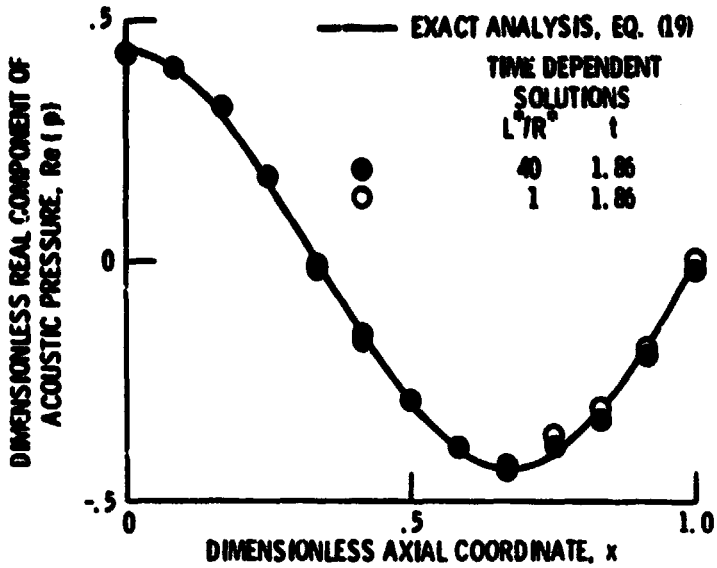

Figure 3. - Analytical and numerical pressure profiles for spinning mode propagation in an infinite hard wall duct at dimensionless frequency $\eta_r = 1.0$, $\xi = 1.5$ ($m = 3$, $n = 0$, $J = 20$, $\Delta x = .0833$, $r = 1$, $C_0^*/C_g^* = 1.345$, $\Delta t = 0.0222$).

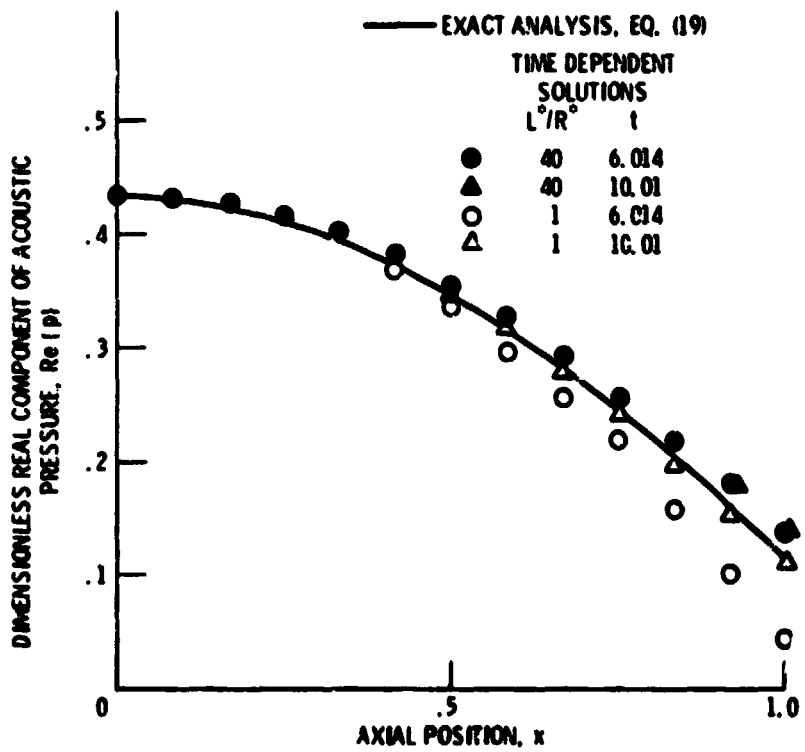

Figure 4. - Analytical and numerical pressure profiles for spinning mode propagation in an infinite hard wall duct with dimensionless frequency $\eta_r = 0.7$, $\xi = 1.047$ ($m = 3$, $n = 0$, $J = 20$, $\Delta x = .0833$, $r = 1$, $C_0^*/C_g^* = 2.365$, $\Delta t = 0.015540$).

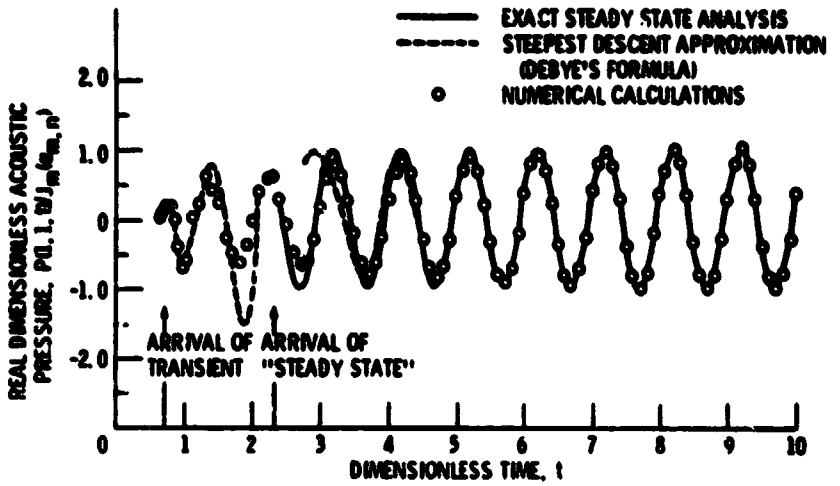

Figure 5. - Analytical and numerical time pressure profiles at x = 1, r = 1 for spinning mode (m = 3) propagating in an infinite hard wall duct with $\eta_r = 0.7$, $\zeta = 1.047$.

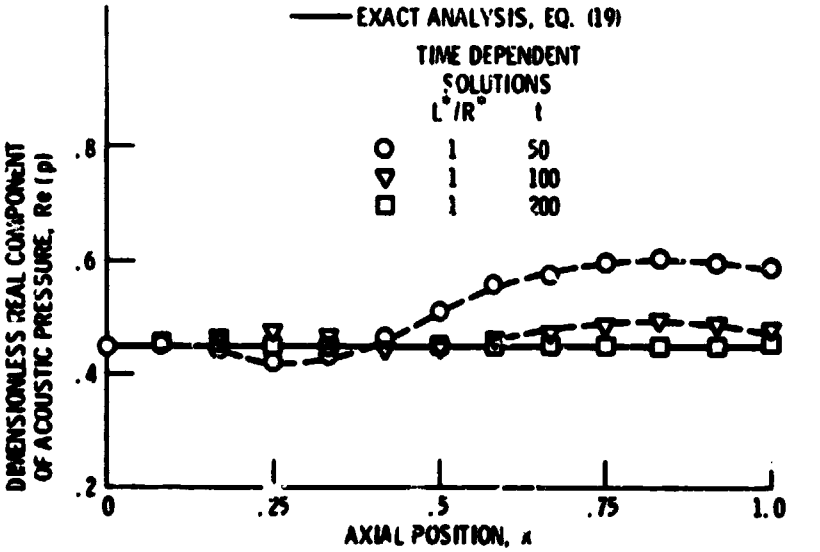

Figure 6. - Analytical and numerical pressure profiles for spinning mode propagating in an infinite hard wall duct with $\eta_r = 0.6687$, $\zeta = 1.00009$ (m = 3, n = 0, J = 20, $\Delta x = 0.0833$, r = 1, $C_0^*/C_g^* = 49.98$, $\Delta t = 0.01665$).

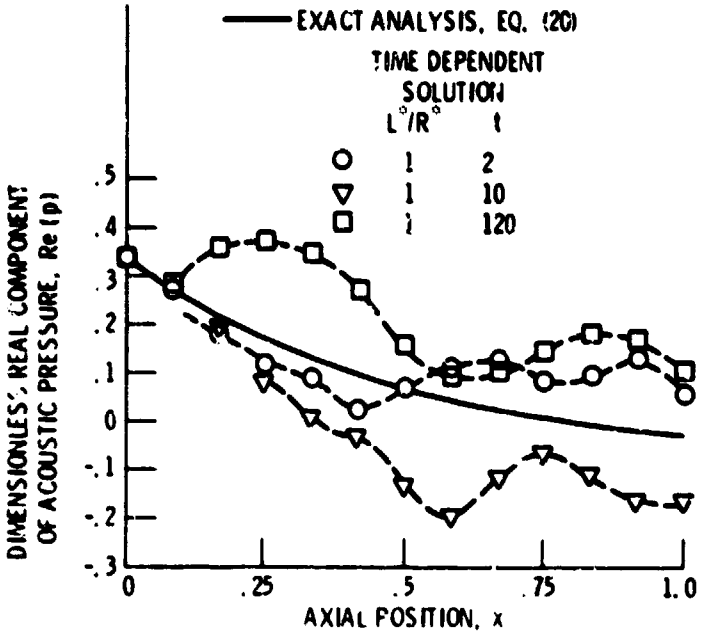

Figure 7. - Analytical and numerical pressure profiles for a cutoff spinning mode propagating in an infinite hard wall duct with $\eta_r = 0.6$, $\xi = 0.9$ ($m = 3$, $n = 0$, $J = 20$, $\Delta x = 0.0833$, $r = 1$, $\Delta t = 0.01485$).

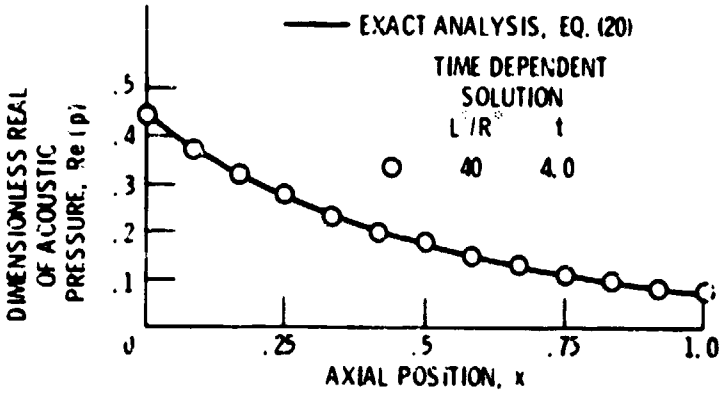

Figure 8. - Analytical and numerical pressure profiles for a cutoff spinning mode propagating in an infinite hard wall duct with $\eta_r = 0.6$, $\xi = 0.9$ ($m = 3$, $n = 0$, $J = 20$, $\Delta x = 0.0833$ $r = 1$, $\Delta t = 0.01332$).

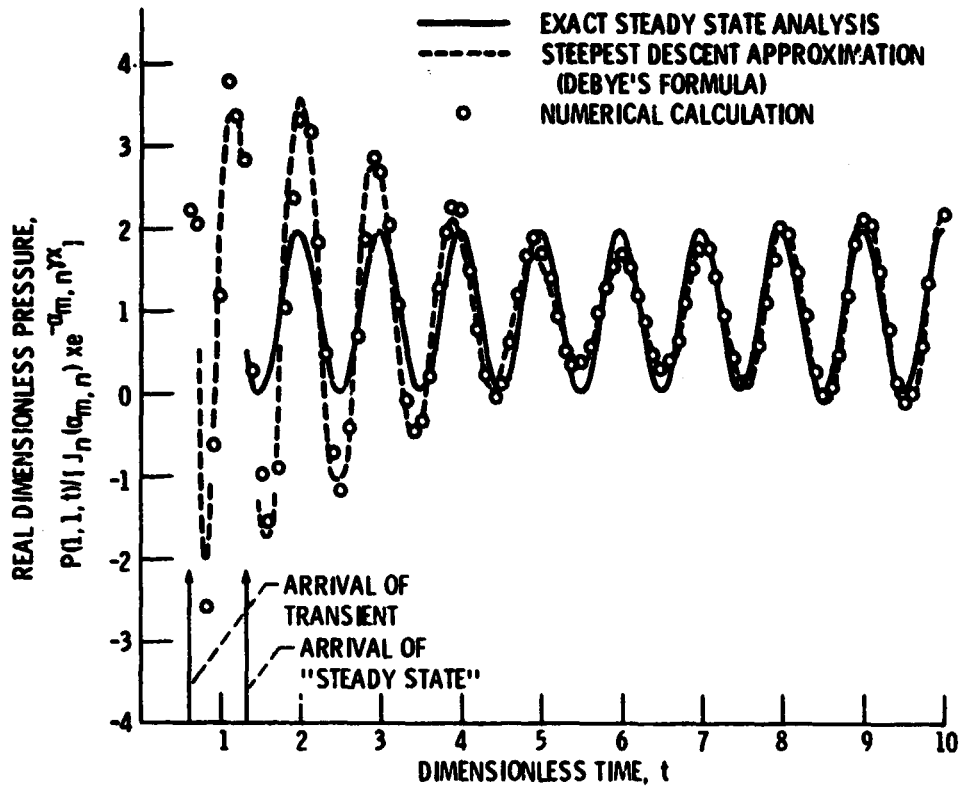

Figure 9. - Analytical and numerical time pressure profiles at x = 1, r = 1 for nonpropagating spinning mode (m = 3) with $\eta_r = 0.6$, $\xi = 0.9$.

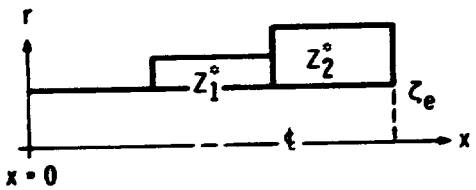

(a) Soft wall duct.

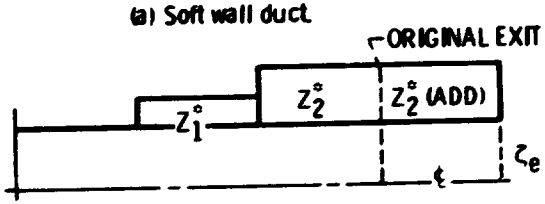

(b) Soft wall duct with liner extension.

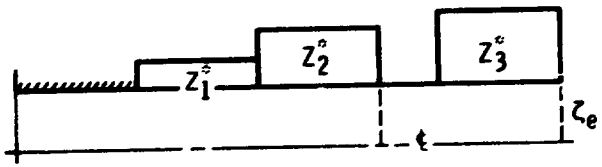

(c) Soft wall duct with liner added downstream of exit.

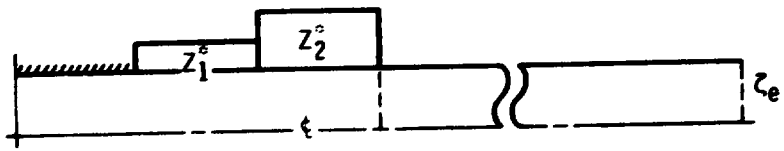

(d) Soft wall duct with semi-infinite exit.

Figure 10. - Exit plane termination impedance models of turbojet engine.

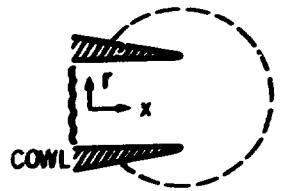

(a) Spherical exit boundary.

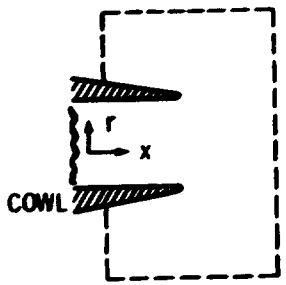

(b) Cylindrical exit boundary.

Figure 11. - Far field radiation exit impedance.